biblio.ugent.be

The UGent Institutional Repository is the electronic archiving and dissemination platform for all UGent research publications. Ghent University has implemented a mandate stipulating that all academic publications of UGent researchers should be deposited and archived in this repository. Except for items where current copyright restrictions apply, these papers are available in Open Access.

This item is the archived peer-reviewed author-version of:

Title: Simulation of hydrogen auto-ignition in a turbulent co-flow of heated air with LES and CMC approach

Authors: I. Stanković, A. Triantafyllidis , E. Mastorakos, C. Lacor, B. Merci

In: Flow, Turbulence and Combustion: Volume 68, Issue 3, 689-710, 2011.

The original publication is available at www.springerlink.com

To refer to or to cite this work, please use the citation to the published version:

I. Stanković, A. Triantafyllidis, E. Mastorakos, C. Lacor, B. Merci. (2011) Simulation of hydrogen auto-ignition in a turbulent co-flow of heated air with LES and CMC approach. *Flow, Turbulence and Combustion*. 86:689-710,2011 (DOI: 10.1007/s10494-010-9277-0)

Noname manuscript No.
(will be inserted by the editor)

Simulation of hydrogen auto-ignition in a turbulent co-flow of heated air with LES and CMC approach

I. Stanković · A. Triantafyllidis · E. Mastorakos · C. Lacor · B. Merci

Abstract Large-Eddy Simulations (LES) with the first order Conditional Moment Closure (CMC) approach of a nitrogen-diluted hydrogen jet, igniting in a turbulent co-flowing hot air stream, are discussed. A detailed mechanism (9 species, 19 reactions) is used to represent the chemistry. Our study covers the following aspects: CFD mesh resolution; CMC mesh resolution; inlet boundary conditions and conditional scalar dissipation rate modelling. The Amplitude Mapping Closure for the conditional scalar dissipation rate produces acceptable results. We also compare different options to calculate conditional quantities in CMC resolution. The trends in the experimental observations are in general well reproduced. The auto-ignition length decreases with an increase in co-flow temperature and increases with increase in co-flow velocity. The phenomena are not purely chemically controlled: the turbulence and mixing play also affect the location of auto-ignition. In order to explore the effect of turbulence, two options were applied: random noise and turbulence generator based on digital filter. It was found that stronger turbulence promotes ignition.

Keywords Conditional Moment Closure · Large Eddy Simulations · Auto-ignition · Hydrogen

1 Introduction

The understanding of the complex interaction between turbulence, molecular diffusion and slow chemistry, leading to auto-ignition, is an important element for the development of many combustion devices (e.g low NOx diesel and homogeneous charge compression injection engines and lean premixed pre-vaporized gas turbines). This motivated Markides and

I. Stanković · B. Merci
Department of Flow, Heat and Combustion Mechanics, Ghent University,
St.-Pietersnieuwstraat 41, 9000 Ghent Belgium
Tel.: +32 9 264 33 00
Fax: +32 9 264 35 75
E-mail: Ivana.Stankovic@UGent.be

A. Triantafyllidis · E. Mastorakos
Hopkinson Laboratory, Engineering Department, Cambridge University

C. Lacor
Department of Mechanical Engineering, Vrije Universiteit Brussel

Mastorakos [1] to perform experiments of the auto-ignition of a hydrogen jet, diluted with nitrogen, issued into a co-flow of pre-heated air at atmospheric pressures. In the experiment, different auto-ignition regimes ("no-ignition" regime, "random spots" regime, flashback, and lifted flame) were obtained by varying the co-flow temperature and velocity. It was shown that the auto-ignition length decreased with an increase in co-flow temperature and increased with increase in co-flow velocity.

In the present study, we combine the Large-Eddy Simulation (LES) technique with the first order Conditional Moment Closure (CMC) [2] approach as turbulent combustion model and we examine the experiment of [1]. In the literature, there are only few LES studies of hydrogen auto-ignition, using the probability density function (PDF) as a sub-grid scale model [3,4], or tabulated chemistry [5]. In [3,4], the ignition length was well reproduced and it was also demonstrated that flashback occurs at high co-flow temperatures. The CMC model has been applied on this test case [1] in the past only in a RANS context [6], without success in reproducing the "random spot" regime (in all cases studied an attached flame was formed). For the n-heptane jet case, in equal velocity conditions in the same geometry, i.e. jet velocity equal to the co-flow velocity, the ignition length was captured well using RANS and CMC [7]. In the context of LES, the CMC model has been used to study methane flames (Sandia D [8], lifted flame stabilized by auto-ignition [9] and bluff-body flames [10,11]) with very good results.

In CMC, transport equations are solved for the conditionally averaged reacting scalars, conditioned on mixture fraction, a conserved scalar. When CMC is used, it is common practice to use a dual mesh approach, where the CMC grid is coarser than LES one. A coarse spatial grid can be used in CMC since the conditional mean quantities have weaker spatial dependence than unconditional quantities. This reduces the computational cost of a simulation. As the CMC equations require flow-field information obtained from the LES (mixture fraction, velocity, scalar dissipation rate and diffusivity), an averaging procedure has to be used. This is discussed in Section 2.2. Another important aspect is the modelling of the conditional scalar dissipation rate, since it has an important effect on auto-ignition [12].

The specific objectives of the present paper are twofold. First, we investigate the effect of numerical accuracy and model options:

- qualitative appreciation of the simulation results when the LES/CMC methodology is applied to the auto-ignition test case of [1];
- study of the influence of the CFD grid resolution;
- investigation of the influence of the CMC mesh resolution in physical space;
- examination of the influence of the turbulence inlet boundary conditions;
- study of the impact of the model for the conditional scalar dissipation rate.

Second, we study the effect of variations in boundary conditions:

- co-flow temperature;
- co-flow air velocity.

Due to a lack of available experimental data, the comparison with the experiment is limited to the ignition length.

2 Modelling

2.1 Large Eddy Simulations

In LES, only the large energy-containing scales, are resolved, while modelling is applied to represent the effect of the smaller unresolved scales, which contain only a small fraction of the turbulent kinetic energy. The Favre-filtered continuity and Navier-Stokes equations are:

$$\frac{\partial \bar{\rho}}{\partial t} + \frac{\partial (\bar{\rho}\widetilde{u}_i)}{\partial x_i} = 0 \tag{1}$$

$$\frac{\partial (\bar{\rho}\widetilde{u}_i)}{\partial t} + \frac{\partial (\bar{\rho}\widetilde{u}_i\widetilde{u}_j)}{\partial x_j} = -\frac{\partial \bar{p}}{\partial x_i} + \frac{\partial \widetilde{\tau}_{ij}}{\partial x_j} - \frac{\partial \tau_{ij}^{sgs}}{\partial x_j} \tag{2}$$

where $\bar{\rho}$ is the resolved density, $\widetilde{\tau}_{ij}$ is resolved stress tensor and $\tau_{ij}^{sgs} = \bar{\rho}(\widetilde{u_i u_j} - \widetilde{u}_i\widetilde{u}_j)$ is the sub-grid scale stress tensor. The momentum equations can be further elaborated, approximating the resolved stress tensor:

$$\widetilde{\tau}_{ij} = \bar{\mu}\left(\frac{\partial \widetilde{u}_i}{\partial x_j} + \frac{\partial \widetilde{u}_j}{\partial x_i} - \frac{2}{3}\frac{\partial \widetilde{u}_k}{\partial x_k}\delta_{ij}\right) \tag{3}$$

The sub-grid scale stresses are closed with the standard Smagorinsky model [13]:

$$\tau_{ij}^{sgs} - \frac{1}{3}\tau_{kk}^{sgs}\delta_{ij} = -2\mu_t\left(\widetilde{S}_{ij} - \frac{1}{3}\widetilde{S}_{mm}\delta_{ij}\right) = -2\bar{\rho}(C_s\Delta)^2\left|\widetilde{S}\right|\left(\widetilde{S}_{ij} - \frac{1}{3}\widetilde{S}_{mm}\delta_{ij}\right) \tag{4}$$

where $\widetilde{S}_{ij} = (1/2)\left(\partial\widetilde{u}_i/\partial x_j + \partial\widetilde{u}_j/\partial x_i\right)$ is the filtered rate-of-strain tensor and the characteristic filtered rate of strain is $\left|\widetilde{S}\right| = \left(2\widetilde{S}_{ij}\widetilde{S}_{ij}\right)^{1/2}$. The model constant, C_s, is fixed; $C_s = 0.1$ is used. The filter width is defined as $\Delta = (\Delta_x\Delta_y\Delta_z)^{1/3}$.

A transport equation for the filtered mixture fraction $\widetilde{\xi}$ is also solved:

$$\frac{\partial (\bar{\rho}\widetilde{\xi})}{\partial t} + \frac{\partial (\bar{\rho}\widetilde{u}_j\widetilde{\xi})}{\partial x_j} = \frac{\partial}{\partial x_j}\left(\bar{\rho}D\frac{\partial \widetilde{\xi}}{\partial x_j} - \bar{\rho}J_j^{sgs}\right) \tag{5}$$

In equation (5) the unknown term J_j^{sgs}, which represents scalar transport due to sub-grid scale fluctuations, must be modelled. It is modelled similarly to the sub-grid scale stress tensor i.e. $J_j^{sgs} = -D_t\partial\widetilde{\xi}/\partial x_j$. We assume equal diffusivities ($D = \nu/Sc$, $D_t = \nu_t/Sc_t$, $\nu_t = \mu_t/\bar{\rho}$), with a constant Schmidt number ($Sc = Sc_t = 0.7$) and we also assume unity Lewis number.

The mixture fraction variance is obtained from a gradient type model [14]:

$$\widetilde{\xi''^2} = C\Delta^2\frac{\partial \widetilde{\xi}}{\partial x_k}\frac{\partial \widetilde{\xi}}{\partial x_k} \tag{6}$$

where C is a coefficient with a constant value ($C = 0.1$).

The unconditional scalar dissipation rate is modeled according to [14, 15] derived from a equilibrium hypothesis:

$$\widetilde{N} = \left(\frac{\nu}{Sc} + \frac{\nu_t}{Sc_t}\right)\frac{\partial \widetilde{\xi}}{\partial x_k}\frac{\partial \widetilde{\xi}}{\partial x_k} \tag{7}$$

Equation (7) therefore gives the total (resolved plus estimated sub-grid scale) scalar dissipation rate.

2.2 Conditional Moment Closure

In the CMC method [2], transport equations are solved for the conditionally filtered reacting scalars, conditioned on the mixture fraction, ξ. The conditional mean or first conditional moment of reactive scalar of the α-species, Y_α, is defined as:

$$Q_\alpha \equiv \widetilde{Y_\alpha|\eta} = \widetilde{Y}_{\alpha,\eta}, \alpha = 1,...n \tag{8}$$

where η is the sample space variable for ξ (mixture fraction) and the operator $\cdot|\eta$ denotes the fulfillment of the condition on the right hand side of the vertical bar. The conditional fluctuations around the conditional mean are neglected in the first order CMC. The unconditional and conditional filter values are related by:

$$\widetilde{Y}_\alpha = \int_0^1 \widetilde{Y_\alpha|\eta}\widetilde{P}(\eta)d\eta \tag{9}$$

The density-weighted filtered PDF ($\widetilde{P}(\eta)$) is assumed to have a β-shape and is calculated from the resolved and sub-grid scale variance of the mixture fraction (equations (5) and (6)).

The CMC transport equations for the conditionally filtered reactive scalars, Q_α, read [8]:

$$\frac{\partial Q_\alpha}{\partial t} + \underbrace{\widetilde{u_i|\eta}\frac{\partial Q_\alpha}{\partial x_i}}_{T_1} - \underbrace{\widetilde{N|\eta}\frac{\partial^2 Q_\alpha}{\partial \eta^2}}_{T_2} = \underbrace{\widetilde{W_\alpha|\eta}}_{T_3} + \underbrace{e_Y}_{T_4}, \ \alpha = 1,...,n \tag{10}$$

The equations are solved for the n species of the reaction mechanism. The first term on the left-hand side of equation (10) is the unsteady term. The second term (term T1) represents the transport by convection through the conditional velocity. The last term on the left-hand side (term T2) represents diffusion in mixture fraction space. The first term on the right-hand side (term T3) is the conditional chemical source term. The last term on the right-hand side, i.e. the sub-grid scale conditional flux, (term T4) accounts for the conditional transport in physical space.

Additionally to the solution of the transport equations for the conditional mean species mass fractions, the transport equation for the conditional mean temperature is solved, ignoring radiation and pressure work [16]:

$$\frac{\partial Q_T}{\partial t} + \underbrace{\widetilde{u_i|\eta}\frac{\partial Q_T}{\partial x_i}}_{T_1} - \underbrace{\widetilde{N|\eta}\left[\frac{1}{c_{p_\eta}}\left(\frac{\partial c_{p_\eta}}{\partial \eta} + \sum_{\alpha=1}^{n} c_{p_{\alpha_\eta}}\frac{\partial Q_\alpha}{\partial \eta}\right)\frac{\partial Q_T}{\partial \eta} + \frac{\partial^2 Q_T}{\partial \eta^2}\right]}_{T_2} =$$

$$\underbrace{-\frac{1}{c_{p_\eta}}\sum_{\alpha=1}^{n} h_\alpha \widetilde{W_\alpha|\eta}}_{T_3} \underbrace{-\frac{\nabla\cdot(\bar{\rho}\widetilde{\mathbf{u}''T''|\eta}\widetilde{P}(\eta))}{\bar{\rho}\widetilde{P}(\eta)}}_{T_4} \tag{11}$$

The main advantage of the CMC approach is that the conditional fluctuations are much smaller than unconditional fluctuations. Therefore, a first order closure of the conditional chemical source term can often be applied, using the mean conditionally filtered reacting scalars:

$$\widetilde{W_\alpha|\eta} = W_\alpha(Q_\alpha, Q_T) \tag{12}$$

We adopt this approach here. The chemical mechanism used here is described in Section 4.1.

The unclosed terms in equations (10) and (11) are the term e_Y, the conditionally filtered velocities ($\widetilde{u_i|\eta}$) and the conditionally filtered scalar dissipation rate ($\widetilde{N|\eta}$). These terms rely on flow-field information, obtained from the LES. The term e_Y is modeled with the gradient diffusion approach [8]:

$$e_Y = -\frac{\nabla\cdot(\bar{\rho}\widetilde{\mathbf{u}''Y_\alpha''|\eta}\widetilde{P}(\eta))}{\bar{\rho}\widetilde{P}(\eta)} \approx \nabla\cdot(D_{t_\eta}\nabla Q_\alpha) + \frac{D_{t_\eta}}{\bar{\rho}\widetilde{P}(\eta)}\nabla Q_\alpha\cdot\nabla\bar{\rho}\widetilde{P}(\eta) \tag{13}$$

where D_{t_η} is the sub-grid scale turbulent diffusivity.

The conditionally filtered scalar dissipation rate can be modelled with the Amplitude Mapping Closure (AMC) [17]:

$$\widetilde{N|\eta} = \frac{\widetilde{N}G(\eta)}{\int_0^1\widetilde{P}(\eta)G(\eta)d\eta}$$

$$G(\eta) = exp(-2[erf^{-1}(2\eta-1)]^2) \tag{14}$$

where $\widetilde{N}$ is the resolved plus sub-grid scale unconditional scalar dissipation rate (equation (7)). In the AMC model as described, the conditional scalar dissipation rate profile as function of mixture fraction is prescribed by the bell-shape of function $G(\eta)$.

In practice, a coarse grid is used to solve equations (10) and (11). This is justified by the weaker spatial dependence of conditional quantities [16]. This implies that averaging is applied to transfer the flow-field information from the LES resolution to the CMC resolution. One of the possibilities is to use mass weighted volume averaging [18]:

$$\widetilde{\psi}^* = \frac{\int\widetilde{\psi}\bar{\rho}dV}{\int\bar{\rho}dV}|_{CFD\in CMC} \tag{15}$$

where $\widetilde{\psi}$ is a scalar calculated in the LES code. Another possibility is to use PDF averaging:

$$\widetilde{\psi|\eta} = \frac{\int\bar{\rho}\widetilde{P}(\eta)\widetilde{\psi|\eta}_{LES}dV}{\int\bar{\rho}\widetilde{P}(\eta)dV}|_{CFD\in CMC} \tag{16}$$

For the conditionally filtered scalar dissipation rate this gives:

$$\widetilde{N|\eta} = \frac{\int\bar{\rho}\widetilde{P}(\eta)\widetilde{N|\eta}_{LES}dV}{\int\bar{\rho}\widetilde{P}(\eta)dV}|_{CFD\in CMC} \tag{17}$$

In equation (17), $\widetilde{N|\eta}_{LES}$ is provided by the AMC model (14) applied to the LES cell. The notation $\cdot|_{CFD\in CMC}$ denotes averaging over all CFD cells within the CMC cell considered. Note that now the shape of the conditional scalar dissipation rate profile is no longer prescribed by $G(\eta)$, but also affected by $\widetilde{P}(\eta)$.

We discuss three options in the paper. In "option 1", we apply mass weighted volume averaging (equation (15)) to the conditionally filtered velocity as:

$$\widetilde{u_i|\eta} = \widetilde{u}_i^* \tag{18}$$

The turbulent diffusivity is evaluated as:

$$D_{t_\eta} = D_t^* \tag{19}$$

also applying mass weighted volume averaging. For the conditional scalar dissipation rate we apply equation (17) (PDF averaging).

In "option 2", mass-weighted volume averaging is applied for the calculation of the conditionally filtered velocity (equation (18)), turbulent diffusivity (equation (19)) and the unconditional scalar dissipation rate. The AMC model is applied directly to the CMC cells (i.e. first equation (15), then equation (14)).

The third option is to apply simple conditional averaging over all CFD cells within each CMC cell [8]:

$$\widetilde{N|\eta} = \left\langle \widetilde{N}|\eta \right\rangle_{CFD\in CMC};\ \widetilde{u_i|\eta} = \langle \widetilde{u}_i|\eta\rangle_{CFD\in CMC};\ D_{t_\eta} = \langle D_t|\eta\rangle_{CFD\in CMC} \qquad (20)$$

By examining the results obtained for the present auto-ignition problem, which should be sensitive to the scalar dissipation rate [1], we may assess the accuracy expected when using these various options for transferring LES information to the CMC grid.

3 Test Case Description

Fuel is injected into a co-flowing air stream through a 2.25mm (d) diameter nozzle at ambient pressure (Fig. 1). The fuel consists of hydrogen, diluted with nitrogen ($Y_{H_2} = 0.13$ and $Y_{N_2} = 0.87$). The stoichiometric mixture fraction, η_{ST}, is 0.184. The burner inner diameter is 25mm. In the experiments [1], co-flow air velocities (u_{cf}) up to 35m/s, with temperatures (T_{cf}) up to 1015K, have been achieved. The fuel velocity ranged from 20 to 120m/s, with temperatures between 650K and 930K. Air was electrically preheated and flowed into a circular tube, after passing through a perforated plate to promote turbulence. Different auto-ignition regimes (no ignition, random spots, flashback and lifted flame) are obtained by varying the temperature of the air and the inlet air velocity. Regions of presence of OH chemiluminescence were considered as an "auto-ignition spot" [1]. Table 1 summarizes the settings for our numerical simulations.

4 Numerical methods and model options

4.1 Chemical kinetics

The chemical kinetics, leading to ignition, is complex and a detailed chemical mechanism must be used. Here, we use the scheme of [19], which consists of 19 reactions and 9 species (H_2, H, O, O_2, OH, H_2O, HO_2, H_2O_2, and N_2). A two-dimensional DNS study [20] confirmed that the ignition always occurs at the location where the mixture fraction is close to the "most reactive" mixture fraction, η_{MR}. The "most reactive" mixture fraction is defined as a mixture fraction with a optimal composition which is likely to ignite first. At that value of mixture fraction, the reaction rate becomes maximum and scalar dissipation rate is low [12]. We determine η_{MR} with a stand-alone 0D-CMC code. This is equivalent to equation (10), without physical transport terms, i.e. a one dimensional equation in η-space, where the micro-mixing was switched off, using a scalar dissipation rate of $10^{-20}\mathrm{s}^{-1}$, giving thus a parallel solution to a series of homogeneous reactors of varying mixture fraction. The number of nodes in mixture fraction space is 51, as in the 3D-CMC simulations. Two auto-ignition criteria (increase of temperature of 1% over the nominal co-flow temperature [3] and mass fraction of OH reaches 2×10^{-4} [21]) gave the same result. The most reactive

mixture fraction depends on the co-flow temperature (Table 2). It is always located in the very lean side, $\eta_{MR} < \eta_{ST}$.

4.2 Numerical set-up

The flow field solver is an in-house LES code, developed at VUB [22]. In the momentum equations, the convective fluxes are discretized in a central manner (second order spatial accuracy). In the transport equation for mixture fraction, the convective terms are discretized with a second order TVD scheme. In our basic simulations, the solution domain (67.5mm $\times$ 25mm $\times$ 25mm) contains $192 \times 48 \times 48$ CFD cells and we compare to the results obtained on a CFD mesh with $96 \times 48 \times 48$ cells. The implementation is parallel, with 4 blocks in the axial direction. At the inlet of the domain, Dirichlet boundary conditions have been used, imposing the velocity and mixture fraction. At the outlet, Neumann boundary conditions have been applied for all quantities except for pressure, which is imposed (atmospheric pressure).

The CMC code has been developed and validated at Cambridge University [11, 16]. In this code, using the velocity and mixing field as obtained from the flow field solver, transport equations are solved for species mass fractions and temperature, conditioned on mixture fraction. In order to obtain the unconditional mean density, as required for the flow calculations, the conditionally averaged values, obtained from the CMC calculations, are integrated with the mixture fraction PDF (Eq. (9)). As mentioned, we use pre-assumed β-PDF shapes.

A dual mesh approach is used. Thus, each CMC cell contains a number of CFD cells. The basic CMC mesh, covering the same physical space domain as the CFD mesh, consists of $40 \times 4 \times 4$ cells. In order to investigate the influence of the resolution, a finer CMC grid is also used ($80 \times 8 \times 8$ cells). In [23], for the lifted hydrogen jet diffusion flame in cold air, it was shown that the cross-stream dependence of conditional reactive scalars is most notable at the lifted flame base and it becomes negligible downstream. This justifies use of 3D-CMC with a relatively low number of CMC cells in the cross stream directions. The mixture fraction space is discretized into 51 nodes, clustered at the lean side in mixture fraction space, i.e. around the most reactive mixture fraction. In [24], the influence of the resolution in mixture fraction space was investigated and we concluded that, with the clustering at the lean side, this resolution is sufficient.

The turbulence inlet boundary conditions are important. In this flow, the turbulence is dominated by the co-flow, with shear-generated turbulence between the jet and the co-flow to be of some significance only for a short length from the nozzle. We expect the turbulence at the jet inlet to be less important. Therefore, we simply apply random white noise in the jet. We investigate different approaches applied for the co-flow. As basic option, we apply the digital filter of [25]. This technique generates turbulence structures, correlated in time and space, with specified turbulent time and length scales. The procedure starts with the creation of a 3D random field. Convolution with a filter results in a three-dimensional signal (one for each velocity component) with prescribed two point statistics (length scale, energy spectra). In that way, homogeneous turbulence is obtained. The chosen length and time scales are 4.5mm and 1ms, with turbulence intensity 12.5% [1, 5]. A second option is to apply random white noise, although this is known not to describe real turbulence adequately.

Table 3 summarizes all the cases studied at T_{cf} = 945K and co-flow velocity 26m/s.

The general solution strategy is as follows: first, a developed inert turbulent mixing field is computed, from which we start the LES-CMC simulation. At time, t_0, we solve the CMC

equations. After a while, before t_0 + 3.75ms, auto-ignition occurs. We only discuss results in the statistically steady state (t_0 + 20ms). We time-average the results between t_0 + 10ms and t_0 + 20ms. At the inlet, a frozen mixing distribution of reactive scalars was used while adiabatic boundary conditions were used at the walls.

5 Results and Discussion

5.1 Basic flow structure

We first show results for case 1 of Table 3, with T_{cf} = 945K and u_{cf} = 26m/s. Instantaneous resolved temperature fields and species mass fraction fields ($\widetilde{Y}_{OH}$, $\widetilde{Y}_{H}$, $\widetilde{Y}_{H_2}$, $\widetilde{Y}_{H_2O}$, $\widetilde{Y}_{HO_2}$) are shown in Figures 2 and 3 at: t_0 + 10ms and t_0 + 20ms, respectively. As mentioned, the reaction first starts at the so called "most reactive mixture fraction". These first ignition events lead to the small local increase in temperature and subsequently propagate ignition and chemical reaction towards higher values of mixture fraction (not shown). After a sufficiently long distance from the nozzle, the maximum temperature is reached around the stoichiometric mixture fraction (0.184). The maximum flame temperature is around 2400K. For the examined test case, both temperature and OH mass fraction can be used for detection of auto-ignition.

HO_2 is produced during induction time, prior to auto-ignition. The HO_2 radical acts as a precursor to auto-ignition and as combustion proceeds it is mostly consumed, thus seemingly remaining at the flame base. During the auto-ignition process, H_2 and O_2 are also slowly consumed while the concentrations of H, OH, H_2O increase at the ignition location. The highest values of the H radical are found in the rich region, after ignition, while H_2O corresponds to the high temperature region. The hot regions, corresponding to high OH mass fraction, are convected downstream out of the domain.

The auto-ignition phenomena in the test case under study are transient but statistically steady and the average behavior can be studied. In Fig. 4, contours of the time averaged temperature and species mass fraction in physical space are shown. Radially averaged and time averaged conditional temperature and conditional species mass fraction profiles are shown in Fig. 5. Each line in Fig. 5 corresponds to one CMC cell. Time averaging for the LES and CMC results was performed with data being collected over 10ms. A lifted flame is seen with a lift-off height of approximately 19.5mm. The structure is consistent with the experimental results, and the flame structure shows a gradual progression from the inert ("frozen") distribution at the inlet to the "burning" distributions (Figs. 4 and 5).

5.2 Balance of terms in CMC equation

The balance of the individual terms in the CMC equation for $\widetilde{Y_{HO_2}|\eta}$ (equation (10)) and the temperature (equation (11)) is examined here for case 1, in order to discuss the flame stabilization process. The analysis is done at a long time after ignition (t_0 + 20ms). In Fig. 6, the contour of time averaged temperature is given, where positions P0 to P5, marked with vertical lines, denote axial positions for which we show the profiles at one radial location (corresponding to r = 3.0mm, horizontal line in Fig. 6). Point P0 corresponds to the pre-ignition region, point P1 corresponds to a point just before ignition, while point P5 corresponds to a burning flamelet. The points in between show intermediate values. Each of

the terms at the given positions is plotted separately in mixture fraction space for the CMC equation for the conditional temperature (Fig. 7) and the CMC equation for $\widetilde{Y_{HO_2}|\eta}$ (Fig. 8).

In the induction time, point P0, the temperature and HO_2 build-up occurs around the most reactive mixture fraction. Reactions are suppressed by convection (T_1) and the scalar dissipation rate (T_2). In Fig. 7, just before the burning region (P1), the convection (T_1) and the scalar dissipation rate (T_2) are negative and balance the chemistry (T_3). Diffusion in physical space (T_4) is a small term (also further downstream). As we move into the burning region (P2, P3), the chemistry term is orders of magnitude larger than before and balances with convection. Further downstream (P4, P5), the heat release term is again lower and the scalar dissipation rate (T_2) becomes more important, although convection still prevails.

Figure 8, for $\widetilde{Y_{HO_2}|\eta}$, is particularly interesting, as HO_2 is a precursor for auto-ignition. The positive T_3 term, prior to ignition, becomes negative once ignition has occurred. This is clearly seen, e.g. at $\eta = 0.04$: T_3 is positive for P0, P1 and P2, while it is negative further downstream. Also, the motion of the negative T_3 values in mixture fraction space, for P0 to P5, clearly shows the lean and rich fronts propagating after ignition. Build-up of HO_2 ahead of the flame edge and along the most reactive mixture fraction isoline shows that base of the flame is stabilized by auto-ignition (Figs. 3 and 4).

5.3 Influence of the numerical settings

Figure 9 shows the radial variation of the instantaneous conditional temperature profiles at t_0 + 20ms for positions P2 to P5 (see Fig. 6), i.e. at the flame base and further downstream. At the flame base, the radial dependence is significant, a phenomenon that cannot be captured in 1D-CMC simulations [23]. Downstream, the radial dependence is small, hence justifying the relatively low number of CMC cells in the transverse directions.

In Fig. 10, the contours of the time averaged temperature fields for all cases studied are shown. We first examine the effect of the CFD and CMC mesh resolution (cases 1, 2 and 3). Clearly, the CMC mesh resolution strongly affects the lift-off height: case 2 and case 3 give the same value (13.9mm), insensitive to the CFD mesh, while in case 1, the flame is further downstream. Case 1 is in better agreement with the experiments (see below). It is possible that further refinement of the CMC mesh would move the flame even further downstream, but this has not be investigated yet. These observations are attributed to convection and to a lesser extent to (numerical) diffusion in the CMC equations. When volume averaging (equation (15)) is applied, the conditional velocity is affected mostly near the nozzle when there are not enough cells in the jet region. Consequently, the conditional velocity is lower than when a finer CMC mesh (case 1) is used. With finer CMC cells ($80 \times 8 \times 8$), the effect of convection is better captured and CMC predictions are improved. As a TVD scheme is used, the impact of the numerical diffusion is small, but not negligible.

There is also an effect on the conditional scalar dissipation rate. In general, the scalar dissipation rate is higher when a coarser CFD mesh is used. This is demonstrated in Fig. 11, where radially averaged and time averaged conditional scalar dissipation rate profiles are shown. Each line on each graph corresponds to one CMC cell. The CMC mesh does not have a big impact on the scalar dissipation rate (Fig. 11: case 1 and case 2). Thus, use of a coarser CFD mesh results in slightly higher conditional scalar dissipation rate, but this still does not have a strong influence on the auto-ignition location. This confirms that the scalar dissipation rate is less dominant than the convection (in the CMC equations) in the determination of the flame lift-off height.

The influence of the inlet turbulence is investigated comparing case 3 and case 4: a turbulence generator based on the digital filter [25] (case 3) and random white noise (case 4). With more realistic turbulence, turbulent mixing is more intense and ignition occurs earlier. When random white noise is applied, mixing is slower and ignition is delayed, because the 'turbulence' dies due to lack of any temporal and spatial coherence.

Finally, we discuss the three options to transfer information from the LES to the CMC grid (case 3, 5 and 6). For positions A, B and C, we show the conditional temperature and scalar dissipation rate evolution at the centerline (Fig. 12). Options 1 and 2 predict approximately the same lift-off height (Fig. 10). Figure 12 shows that the characteristic bell-shaped profile for the conditional scalar dissipation rate in option 2, indeed does not strongly deviate from the profile obtained with option 1. In particular, at the lean side, the levels are very similar. Option 3, however, leads to strong fluctuations in the scalar dissipation rate. This results locally in spots with very low scalar dissipation rate, earlier auto-ignition [12] and finally an attached flame, what is not in agreement with the experiments. This suggests that, for this problem, simple conditional averaging is not a suitable manner to transfer the fine-grid LES information to the coarse CMC mesh. Mass weighted averaging or PDF integrations are required. In the problem studied, the AMC model for the conditional scalar dissipation rate can be directly applied on the CMC mesh, without strong influence on the simulation results.

5.4 Variation of the inlet temperature and velocity

The inlet fluctuations, the co-flow velocity and the co-flow temperature affect the first emergence of auto-ignition. In order to show the sensitivity of the system to the co-flow temperature, four simulations, using the fine CFD and CMC mesh as in case 1, were carried out with different co-flow temperatures: 935K, 945K, 960K and 980K (Fig. 13). At the lowest temperatures (935K), high-temperature kernels are generated at a certain distance from the nozzle and convected out of the domain. The temperature is too low for the propagating fronts to establish a real lifted flame. Increasing the co-flow temperature results in a change in the flame behavior. The flame propagates and stabilizes closer to the injector, where the local scalar dissipation rate is high but the temperature is also high enough. A higher co-flow temperature is necessary to access the flashback regime where, as soon as the fuel mixture was injected, auto-ignition and flashback occurred, which resulted in a jet diffusion flame stabilized on the injector nozzle. The sensitivity to the co-flow temperature is due to the chemistry. The possible impact of the chemical mechanism on the ignition delay time was presented in [24]. In Fig. 14, the ignition length observed in experiments (L_{min}), is compared with the present simulations. In the experiment, L_{min} is defined as the minimum axial location of an OH spot observed during a data run. If present simulations are shifted 60K the results fit well with the experimental ignition length, but the trend was well captured even without this shift. This discrepancy can be attributed to uncertainties in the chemical mechanism and in the determination of the temperature in the experiment. In [26], it was indeed shown that for the studied configuration the difference in the ignition distance for the different mechanisms can be up to 12 nozzle diameters.

The effect of the co-flow velocity is tested for T_{cf} = 945K and options as in the case 1, Fig. 15. With a higher co-flow velocity influence of the convection becomes stronger in the balancing flame propagation and the flame stabilizes further downstream. The fact that for the same co-flow temperature, a higher co-flow velocity results in delayed auto-ignition, confirms the delaying effect of the air stream on auto-ignition.

6 Conclusions

LES results, with the first order CMC, have been presented for hydrogen auto-ignition in a turbulent co-flow of heated air, using detailed chemistry. The results are qualitatively consistent with experimental data and previous calculations found in the literature. The auto-ignition length decreases with an increase in co-flow temperature and increases with increase in co-flow velocity. Discrepancies in the lift-off height can be attributed to uncertainties in the chemical mechanism. The phenomena are not only chemically controlled but the turbulence and mixing play a role in determining the location of auto-ignition. Build-up of HO_2 ahead of the flame edge and along the most reactive mixture fraction isoline shows that base of the flame is stabilized by auto-ignition. After auto-ignition, lean and rich flame fronts propagate in mixture fraction space.

It was found that using the Amplitude Mapping Closure model for the conditional scalar dissipation rate gives reasonable results. Various sensitivities of the results to the operating conditions and the manner the fine-grid LES information is transfered to the coarser CMC grid are explored and it was found that, for the problem under study, conditional averaging is not a suitable manner to transfer the fine-grid LES information to the coarse CMC mesh. Mass-weighted averaging or PDF integrations are required.

Acknowledgements This work has been funded by FWO-project G.0079.07.

References

1. Markides, C.N., Mastorakos, E.: An experimental study of hydrogen auto-ignition in a turbulent co-flow of heated air. Proc. Combust. Inst. 30, 883-891 (2005)
2. Klimenko, A.Y., Bilger, R.W.: Conditional moment closure for turbulent combustion. Prog. Energy Combust. Sci. 25, 595-687 (1999)
3. Jones, W.P., Navarro-Martinez, S.: Study of hydrogen auto-ignition in a turbulent air co-flow using a large eddy simulation approach. Comput. Fluids 37, 802-808 (2008)
4. Jones, W.P., Navarro-Martinez, S., Rohl, O.: Large eddy simulation of hydrogen auto-ignition with a probability density function method. Proc. Combust. Inst. 31, 1765-1771 (2007)
5. Galpin, J., Angelberger, C., Naudin, A., Vervisch, L.: Large-eddy simulation of H_2-air auto-ignition using tabulated detailed chemistry. J. Turbul. 9, 1-21 (2008)
6. Patwardhan, S.S., Lakshmisha, K.N.: Auto-ignition of turbulent hydrogen jet in a co-flow of heated air. Int. J. Hydrogen Energy 33, 7265-7273 (2008)
7. Markides, C.N., De Paola, G., Mastorakos, E.: Measurements and simulations of mixing and auto-ignition of an n-heptane plume in a turbulent flow of heated air. Exp. Therm. Fluid Sci. 31, 393-401 (2007)
8. Navarro-Martinez, S., Kronenburg, A., Di Mare, F.: Conditional moment closure for large eddy simulations. Flow Turbul. Combust. 75, 245-274 (2005)
9. Navarro-Martinez, S., Kronenburg, A.: LES-CMC simulations of a lifted methane flame. Proc. Combust. Inst. 32, 1509-1516 (2009)
10. Navarro-Martinez, S., Kronenburg, A.: LES-CMC simulations of a turbulent bluff body flame. Proc. Combust. Inst. 31, 1721-1728 (2007)
11. Triantafyllidis, A., Mastorakos, E., Eggels, R.L.G.M.: Large Eddy Simulations of forced ignition of a non-premixed bluff-body methane flame with conditional moment closure. Combust. Flame 156, 2328-2345 (2009)
12. Mastorakos E.: Ignition of turbulent non-premixed flames. Prog. Energy Combust. Sci. 35, 57-97 (2009)
13. Smagorinsky, J.: General circulation experiments with the primitive equations, Mon. Weather Rev. 91, 99-164 (1963)
14. Pierce, C.D., Moin, P.: A dynamic model for subgrid-scale variance and dissipation rate of a conserved scalar. Phys. Fluids 10, 3041-3044 (1998)
15. Girimaji, S.S., Zhou, Y.: Analysis and modelling of subgrid scalar mixing using numerical data, Phys. Fluids 8, 1224-1236 (1996)

16. Wright, Y.M., De Paola, G., Boulouchos K., Mastorakos, E.: Simulations of spray auto-ignition and flame establishment with two-dimensional CMC. Combust. Flame 143, 402-419 (2005)
17. O'Brien, E., Jiang, T.L.: The conditional dissipation rate of an initially binary scalar in homogeneous turbulence. Phys. Fluids 3, 3121-3123 (1991)
18. Triantafyllidis, A., Mastorakos, E.: Implementation issues of the conditional moment closure model in large eddy simulations. Flow Turbul. Combust. 84, 481-512 (2010)
19. Li, J., Zhao, Z., Kazakov A., Dryer, F.L.: An updated comprehensive kinetic model of hydrogen combustion. Inter. J. Chem. Kinet. 36, 566-575 (2004)
20. Mastorakos, E., Baritaud T.A., Poinsot, T.J.: Numerical simulations of auto-ignition in turbulent mixing flows. Combust. Flame 109, 198-233 (1997)
21. Cao, R.R., Pope, S.B., Masri, A.R.: Turbulent lifted flames in a vitiated coflow investigated using joint PDF calculations. Combust. Flame 142, 438-453 (2005)
22. Broeckhoven, T.: LES of turbulent combustion: numerical study and applications. PhD Thesis, VUB, http://mech.vub.ac.be/thermodynamics/phd/list_lacor.htm (2007)
23. Cheng, T.S., Wehrmeyer, J.A., Pitz, R.W.: Conditional analysis of lifted hydrogen jet diffusion flame experimental data and comparasion to laminar flame solutions. Combust. Flame 150, 340-354 (2007)
24. Stanković, I., Triantafyllidis, A., Mastorakos, E., Merci, B.: Study of hydrogen non-premixed auto-ignition in mixture fraction space using detailed mechanisms. 6th Mediterranean Combustion symposium, 7-11 June, Ajaccio, Corsica (2009)
25. Klein, M., Sadiki, A., Janicka, J.: A digital filter based generation of inflow data for spatially developing direct numerical or large eddy simulations. J. Computat. Phys. 186, 652-665 (2003)
26. Lee, C.W., Mastorakos, E.:Transported scalar PDF calculations of autoignition of a hydrogen jet in a heated turbulent co-flow. Combust. Theory Model. 12, 1153-1178 (2008)

Table 1 Boundary conditions for the simulation

	Fuel jet	Co-Flow
Velocity, (m/s)	120	20-35
Temperature, K	691	935-980
Composition	$Y_{H_2} = 0.13$	$Y_{O_2} = 0.233$
	$Y_{N_2} = 0.87$	$Y_{N_2} = 0.767$

Table 2 Most reactive mixture fraction as a function of co-flow temperature, based on homogeneous reactor calculations

T_{cf} [K]	935	945	960	980
η_{MR} [-]	0.0145	0.0190	0.0234	0.0278

Table 3 Cases studied with the options used in the simulations (T_{cf} = 945K, u_{cf} = 26m/s)

	CFD resolution	CMC resolution	Type of the turbulence generation	Type of conditional averaging
Case 1	192x48x48	80x8x8	digital filter	option 1 (Eqs. (17), (18), (19))
Case 2	192x48x48	40x4x4	digital filter	option 1 (Eqs. (17), (18), (19))
Case 3	96x48x48	40x4x4	digital filter	option 1 (Eqs. (17), (18), (19))
Case 4	96x48x48	40x4x4	random noise	option 1 (Eqs. (17), (18), (19))
Case 5	96x48x48	40x4x4	digital filter	option 2 (Eqs. (15), (18), (19))
Case 6	96x48x48	40x4x4	digital filter	option 3 (Eq. (20))

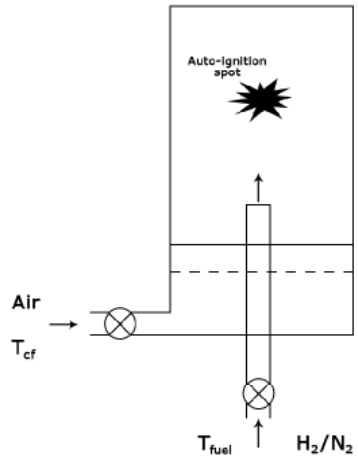

Fig. 1 The experimental set-up of [1]

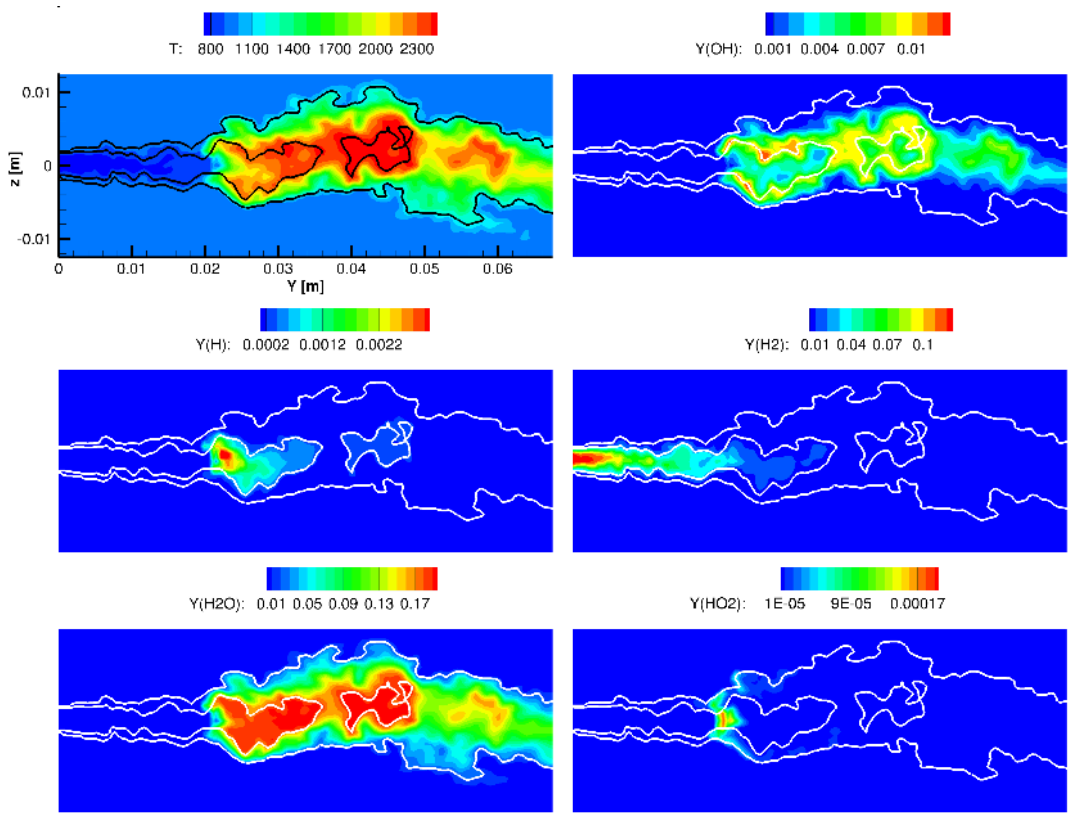

Fig. 2 Instantaneous resolved temperature, $\widetilde{Y}_{OH}$, $\widetilde{Y}_{H}$, $\widetilde{Y}_{H_2}$, $\widetilde{Y}_{H_2O}$ and $\widetilde{Y}_{HO_2}$ fields in a symmetry plane at t_0 + 10ms (case 1). Inner isoline: $\eta_{ST} = 0.184$, outer isoline: $\eta_{MR} = 0.019$

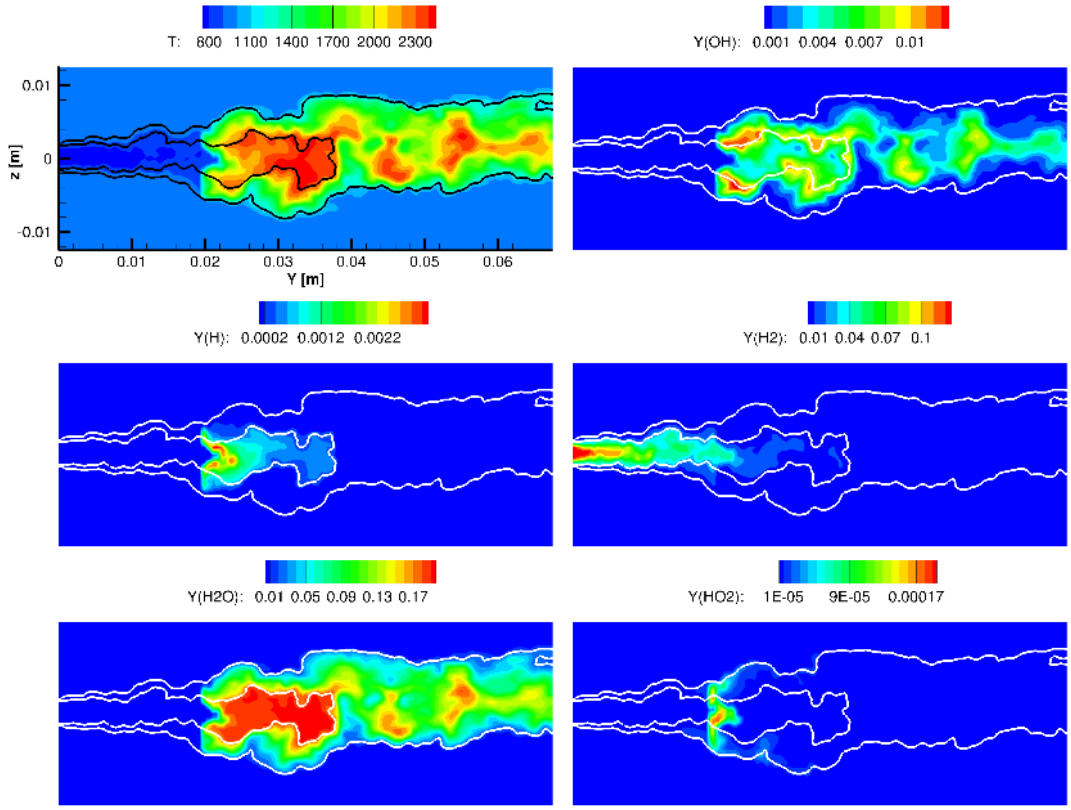

Fig. 3 Instantaneous resolved temperature, $\widetilde{Y}_{OH}$, $\widetilde{Y}_{H}$, $\widetilde{Y}_{H_2}$, $\widetilde{Y}_{H_2O}$ and $\widetilde{Y}_{HO_2}$ fields in a symmetry plane at t_0 + 20ms (case 1). Inner isoline: $\eta_{ST} = 0.184$, outer isoline: $\eta_{MR} = 0.019$

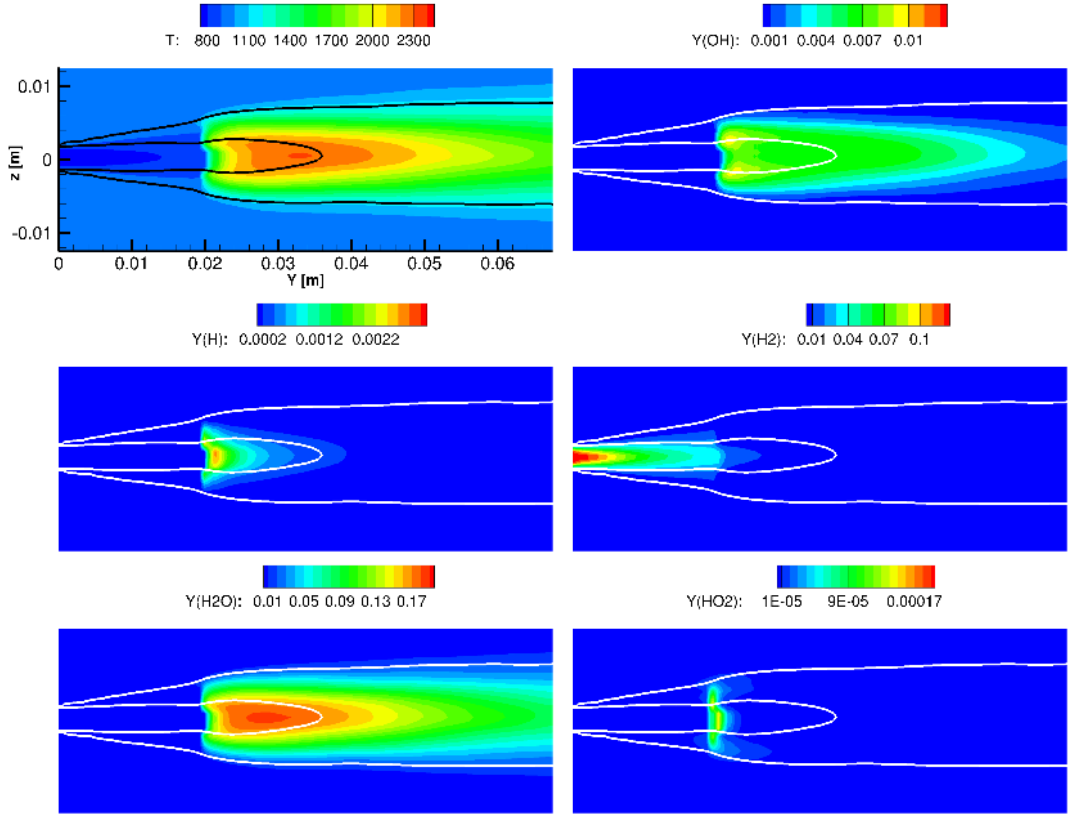

Fig. 4 Contours of the time averaged temperature, $\widetilde{Y}_{OH}$, $\widetilde{Y}_{H}$, $\widetilde{Y}_{H_2}$, $\widetilde{Y}_{H_2O}$ and $\widetilde{Y}_{HO_2}$ fields in a symmetry plane (case 1). Inner isoline: $\eta_{ST} = 0.184$, outer isoline: $\eta_{MR} = 0.019$

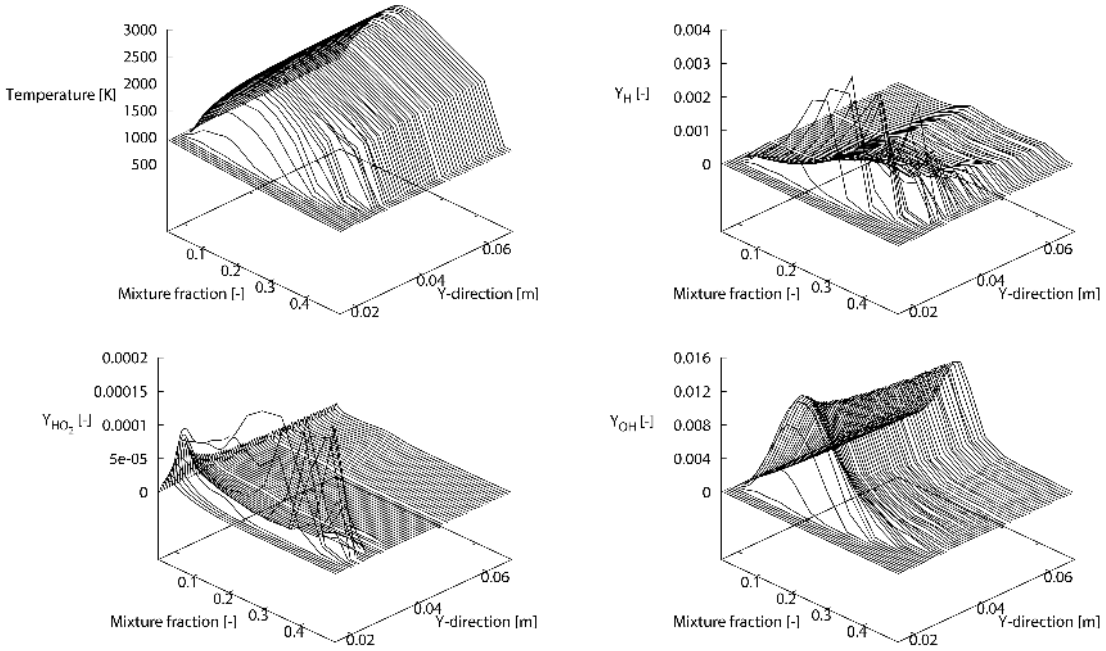

Fig. 5 Time averaged conditional temperature, $\widetilde{Y_{OH}|\eta}$, $\widetilde{Y_H|\eta}$ and $\widetilde{Y_{HO_2}|\eta}$ as a function of mixture fraction (case 1)

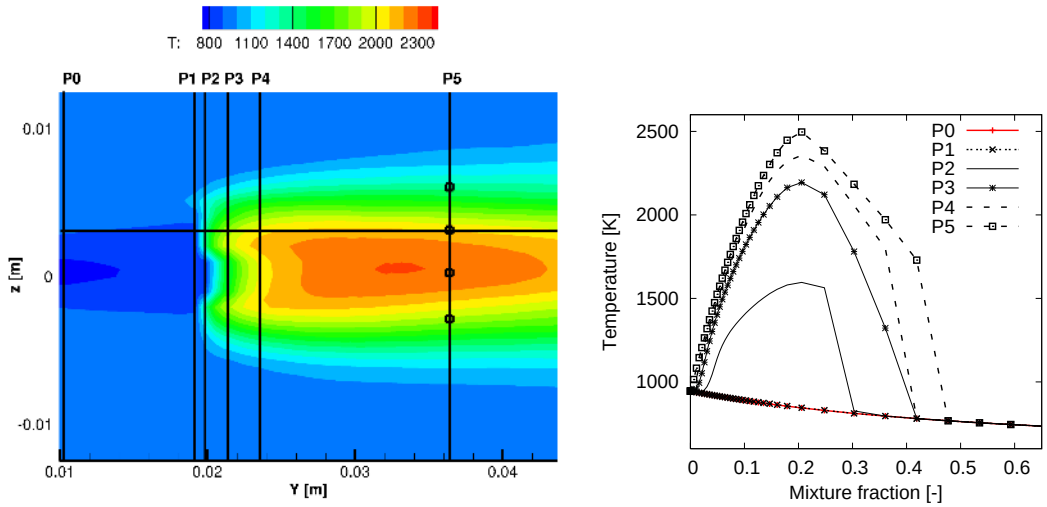

Fig. 6 Contour of the time averaged temperature in K (left) and conditional temperature (right) at $r = 3.0$mm (case 1)

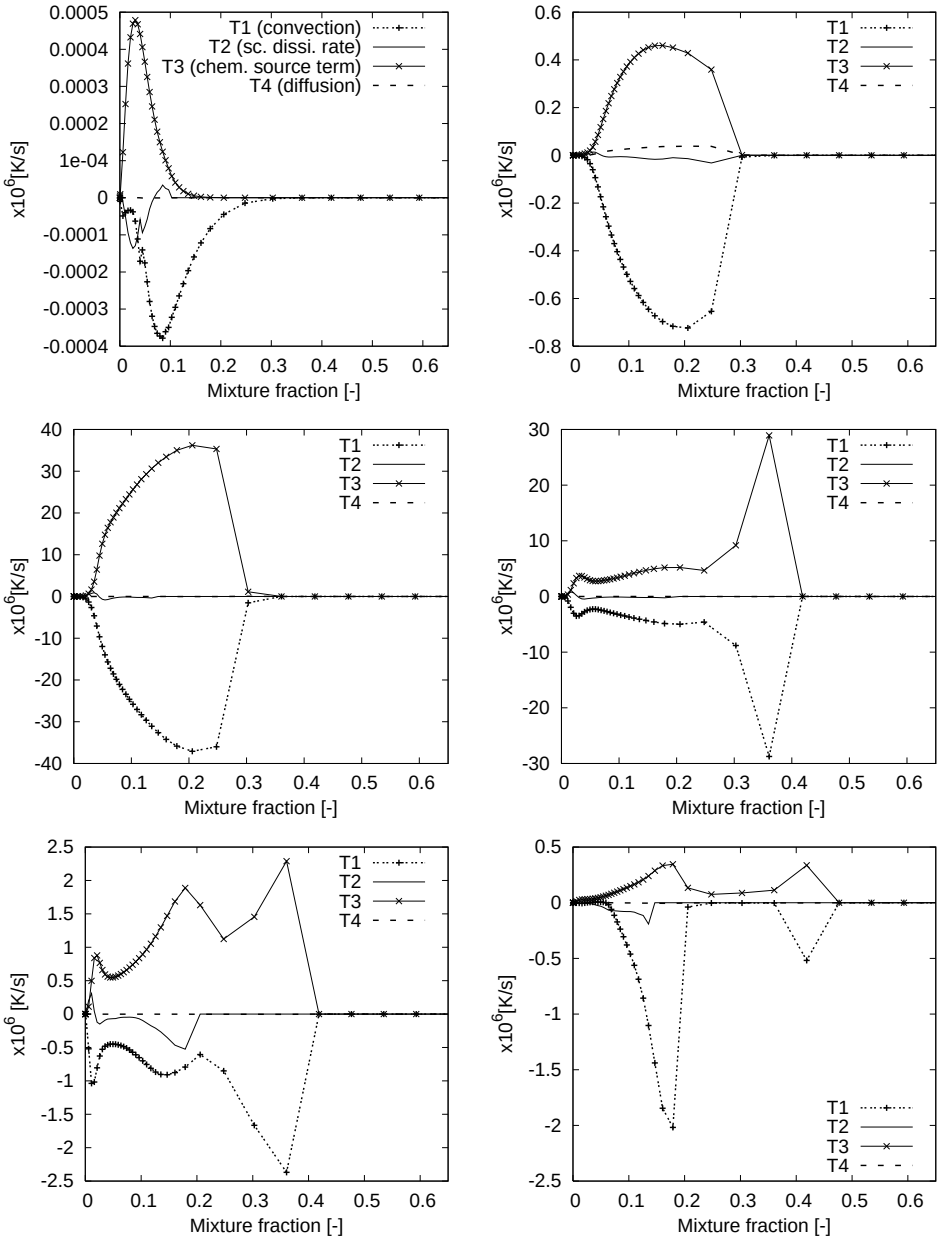

Fig. 7 The terms in the CMC equation Eq. (11) for the conditional temperature at the location P0 (top left), P1 (top right), P2 (middle left), P3 (middle right), P4 (bottom left) and P5 (bottom right). The corresponding locations (P0-5) are indicated in Figure 6 (case 1)

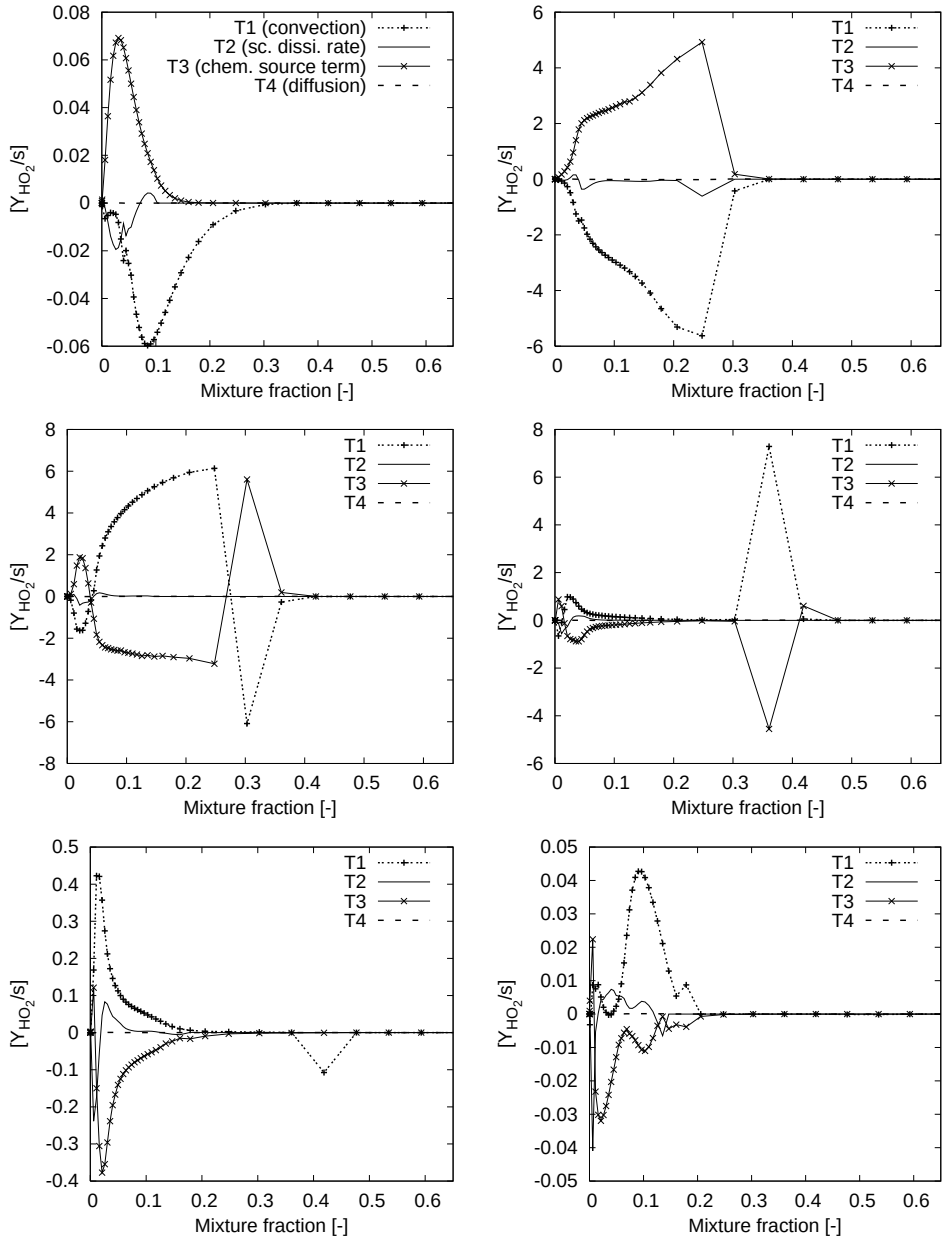

Fig. 8 The terms in the CMC equation Eq. (10) for $\widetilde{Y_{HO_2}|\eta}$ at the location P0 (top left), P1 (top right), P2 (middle left), P3 (middle right), P4 (bottom left) and P5 (bottom right). The corresponding locations (P0-5) are indicated in Figure 6 (case 1)

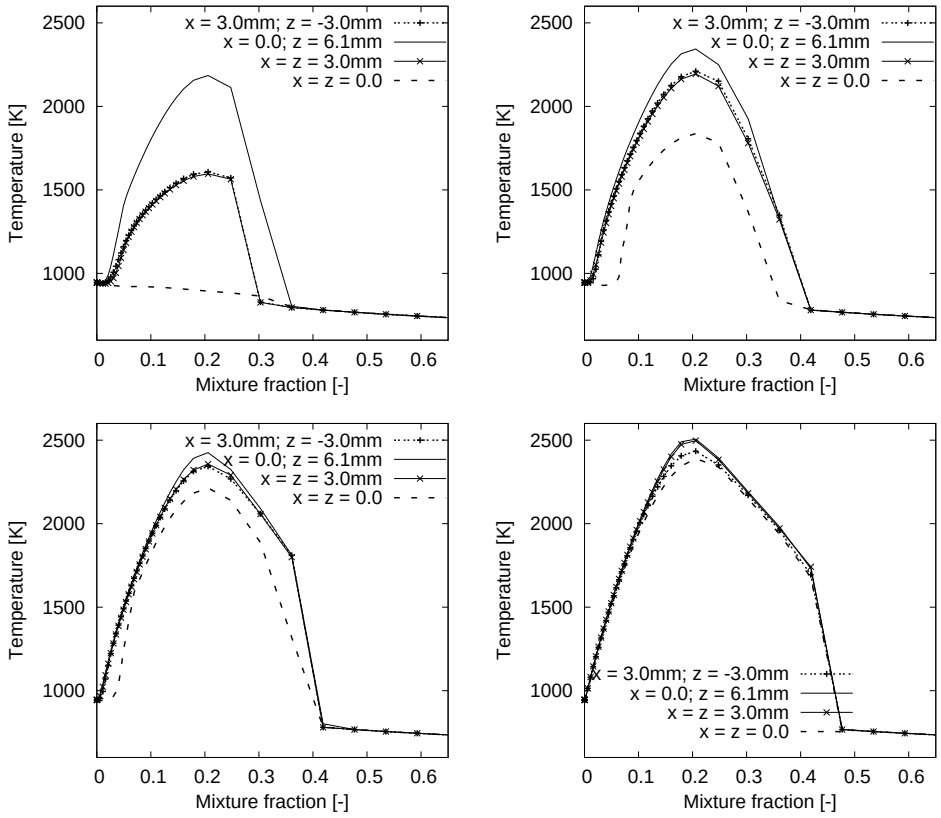

Fig. 9 Conditional temperature at different axial positions (top left: P2, top right: P3, down left: P4 and down right: P5) for four different radial locations. The corresponding axial locations (P2 to 5) and radial (squares) are indicated in Figure 6 (case 1)

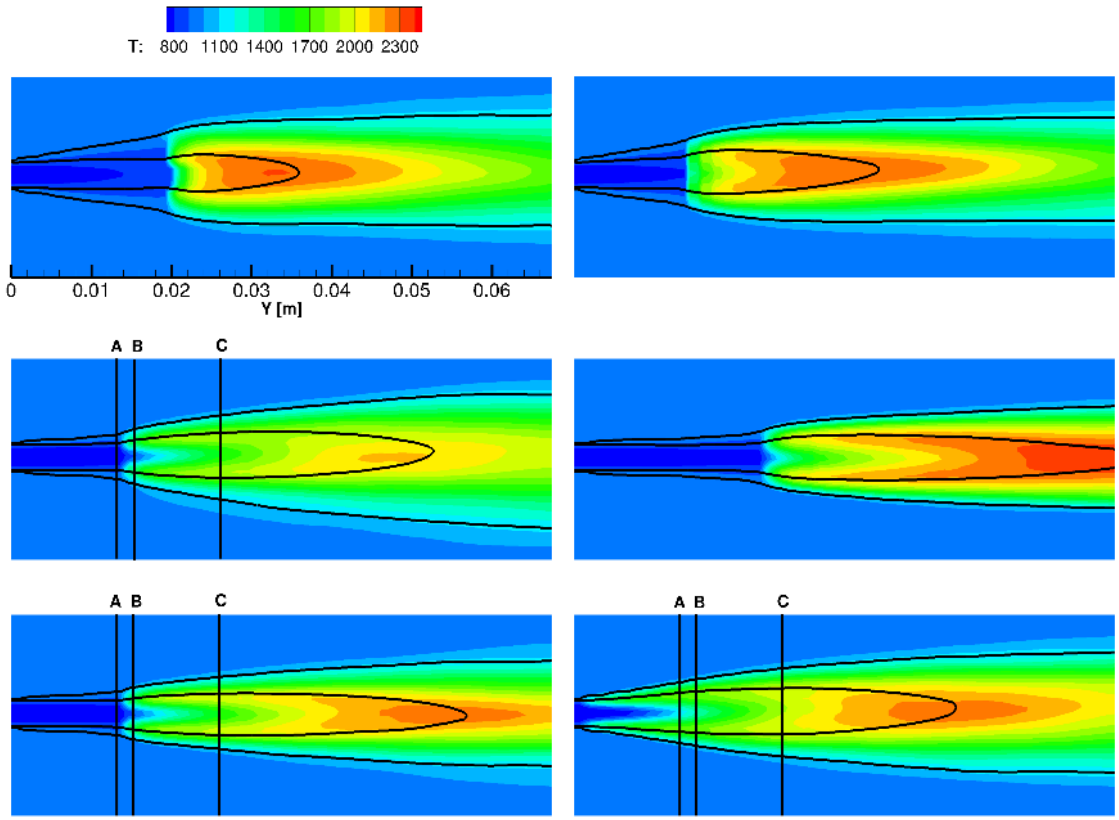

Fig. 10 Contours of the time averaged temperature in a symmetry plane for case 1 (top left), case 2 (top right), case 3 (middle left), case 4 (middle right), case 5 (bottom left) and case 6 (bottom right). The black lines denote the contours of time averaged $\widetilde{\xi} = \eta_{MR}$ and $\widetilde{\xi} = \eta_{ST}$

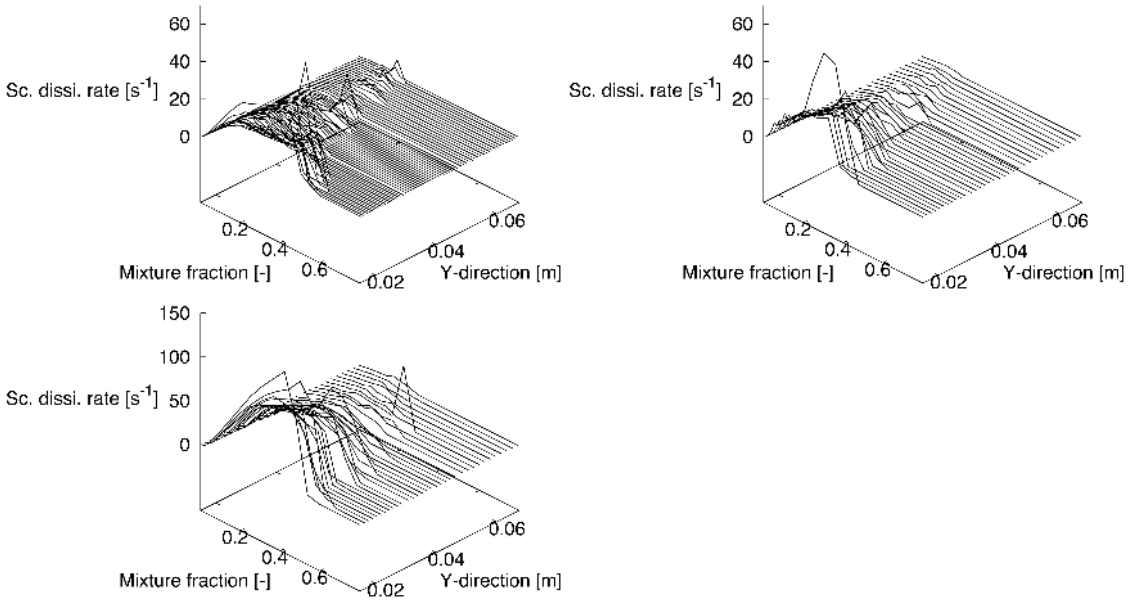

Fig. 11 Time averaged conditional scalar dissipation rate ($\widetilde{N|\eta}$) for case 1 (top left), case 2 (top right), case 3 (bottom)

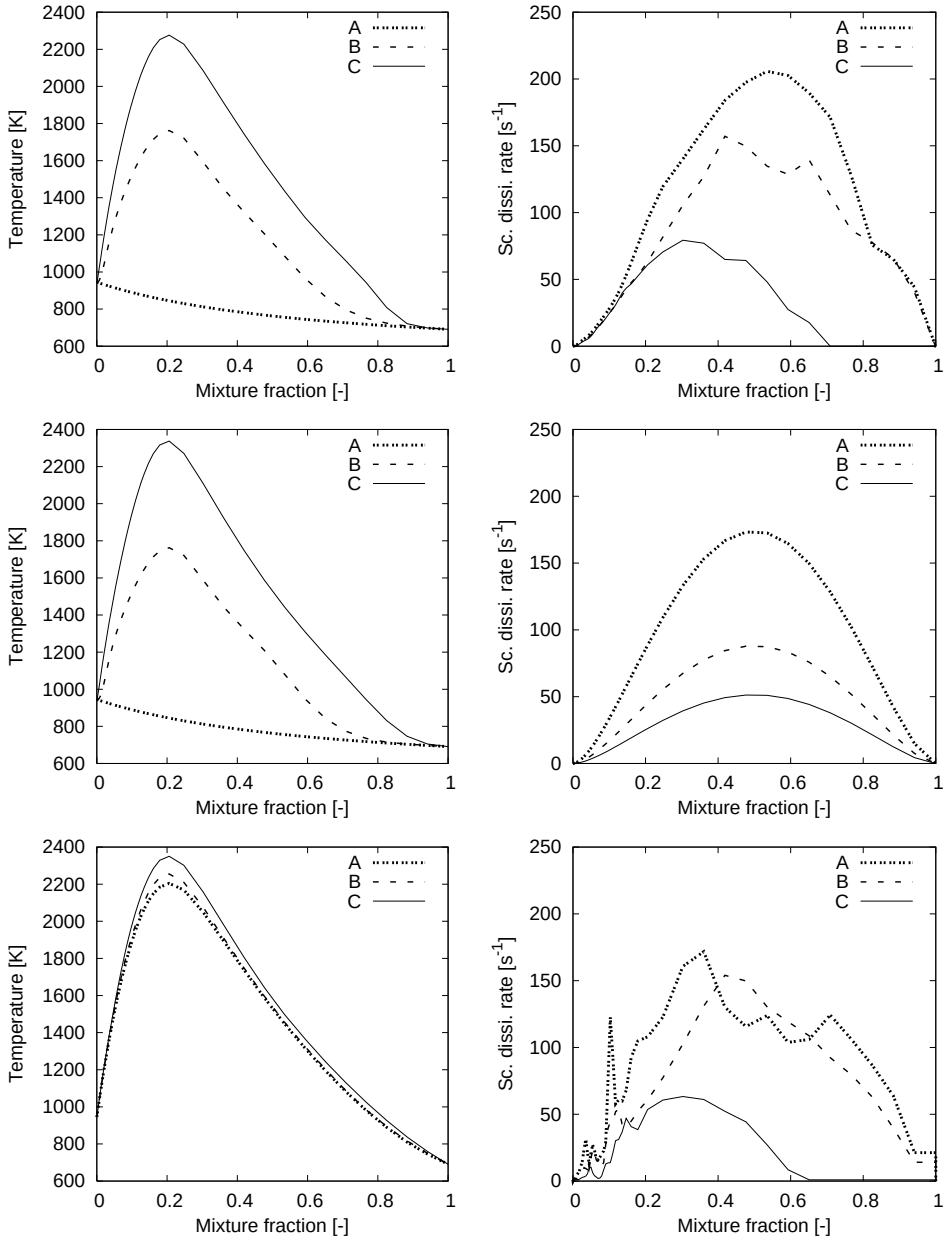

Fig. 12 Conditional temperature (left) and scalar dissipation rate (right) profiles in mixture fraction space for case 3 (top), case 5 (middle) and case 6 (bottom) at the centerline. The corresponding axial locations (A, B and C) are indicated in Figure 10

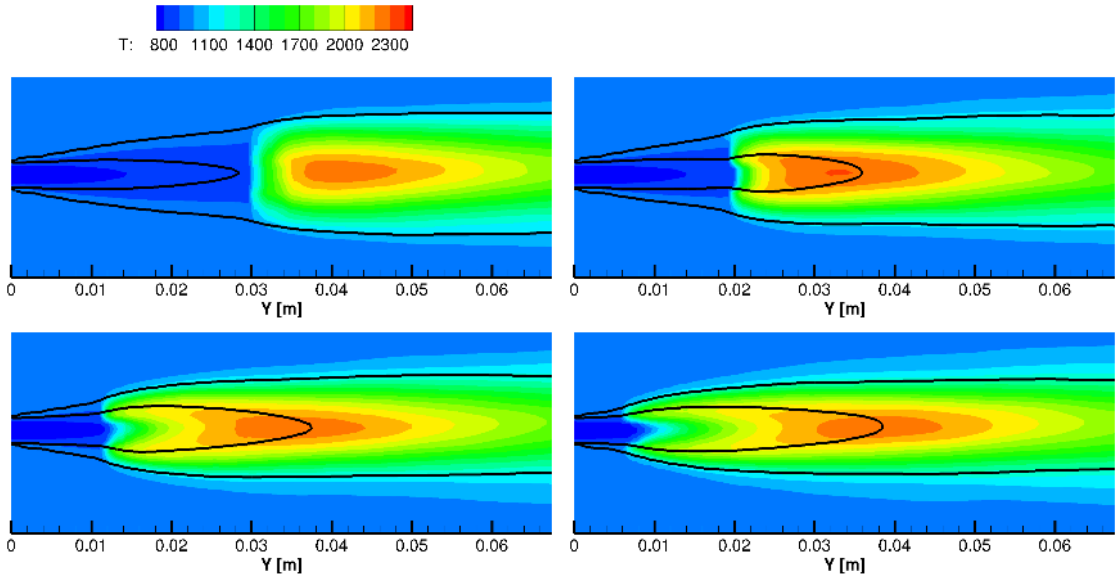

Fig. 13 Contours of the time averaged temperature in a symmetry plane with different co-flow temperatures: 935K (top left), 945K (top right), 960K (down left) and 980K (down right). Inner isoline: η_{ST}, outer isoline: η_{MR} (options as in case 1)

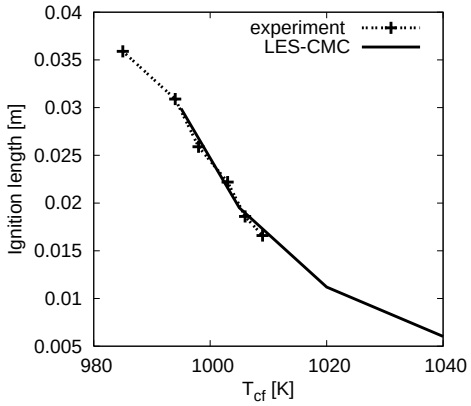

Fig. 14 Comparison of auto-ignition length from experiments (L_{min}) and present calculations (shifted by 60K), options as in case 1

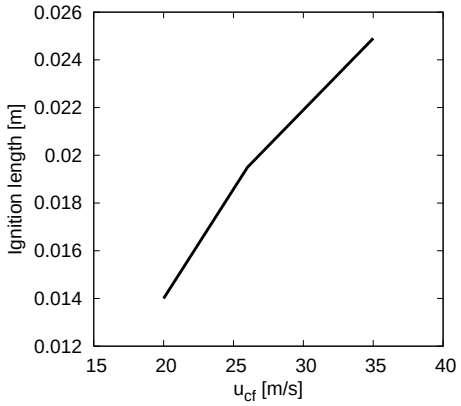

Fig. 15 Auto-ignition length as a function of the co-flow velocity (options as in case 1)